Formation of Toxic Unsaturated Multifunctional and Organosulfur Compounds From the Photosensitized Processing of Fluorene and DMSO at the Air-Water Interface

Majda Mekic, Jiafa Zeng, Bin Jiang, Xue Li, Yannis G Lazarou, Marcello Brigante, Hartmut Herrmann, Sasho Gligorovski

JGR Atmospheres

RESEARCH ARTICLE
10.1029/2019JD031839

Key Points:
- Polycyclic aromatic hydrocarbons can initiate photosensitized chemistry at the air-water interface
- Unsaturated multifunctional compounds are formed in gas and aqueous phases which are known precursors of secondary organic aerosols
- Excited triplet states of PAHs react with dimethyl sulfoxide at the sea surface and lead to formation of S-containing organic compounds

Supporting Information:
- Supporting Information S1

Correspondence to:
H. Herrmann and S. Gligorovski,
gligorovski@gig.ac.cn;
herrmann@tropos.de

Citation:
Mekic, M., Zeng, J., Jiang, B., Li, X., Lazarou, Y. G., Brigante, M., et al. (2020). Formation of toxic unsaturated multifunctional and organosulfur compounds from the photosensitized processing of fluorene and DMSO at the air-water interface. *Journal of Geophysical Research: Atmospheres*, *125*, e2019JD031839. https://doi.org/10.1029/2019JD031839

Received 17 OCT 2019
Accepted 21 FEB 2020
Accepted article online 25 FEB 2020

Formation of Toxic Unsaturated Multifunctional and Organosulfur Compounds From the Photosensitized Processing of Fluorene and DMSO at the Air-Water Interface

Majda Mekic[1,2], Jiafa Zeng[3], Bin Jiang[1], Xue Li[3], Yannis G. Lazarou[4], Marcello Brigante[5], Hartmut Herrmann[6,7,8], and Sasho Gligorovski[1]

[1]State Key Laboratory of Organic Geochemistry, Guangzhou Institute of Geochemistry, Chinese Academy of Sciences, Guangzhou, China, [2]University of Chinese Academy of Sciences, Beijing, China, [3]Institute of Mass Spectrometry and Atmospheric Environment, Jinan University, Guangzhou, China, [4]Institute of Nanoscience and Nanotechnology, National Center for Scientific Research "Demokritos", Agia Paraskevi, Greece, [5]Université Clermont Auvergne, CNRS, SIGMA Clermont, Institut de Chimie de Clermont-Ferrand, Clermont-Ferrand, France, [6]School of Environmental Science and Engineering, Shandong University, Qingdao, China, [7]Shanghai Key Laboratory of Atmospheric Particle Pollution and Prevention, Department of Environmental Science and Engineering, Institute of Atmospheric Sciences, Fudan University, Shanghai, China, [8]Atmospheric Chemistry Department (ACD), Leibniz-Institute for Tropospheric Research (TROPOS), Leipzig, Germany

Abstract Polycyclic aromatic hydrocarbons and dimethyl sulfoxide (DMSO) are ubiquitous at the sea surface. Photochemistry at the air-sea interface is a potentially important source of volatile organic compounds, but the relevant chemical processes are currently not well known. When aqueous solutions containing a mixture of fluorene (FL) and DMSO are irradiated with actinic radiation, a large suite of unsaturated high molecular weight compounds appear in the aqueous phase; a broad variety of saturated and unsaturated oxygenated multifunctional compounds are also observed in the gas phase, most of which are more toxic than FL. A possible sequence of steps leading to some of the observed compounds in aqueous solution as well as in the gas phase is proposed. The reaction pathways initiated by excited triplet state of FL (^{3}FL*) are supported by theoretical calculations of the reaction Gibbs energies. The formation of organosulfur compounds has been observed to occur in the gas and the aqueous phases initiated by the reaction between ^{3}FL* and DMSO. The aforementioned photosensitized chemistry at the water surface can have an important impact on the formation of secondary organic aerosol in marine boundary layer as polycyclic aromatic hydrocarbons and DMSO enriched at the water surface are ubiquitous.

1. Introduction

The sea surface microlayer (SML) is an important interface between the atmosphere and the sea (Donaldson & George, 2012). Presently ongoing environmental changes such as global warming, ocean acidification, and air pollution influence the chemical processes at the SML and thus change the interactions between the upper sea level and lower marine atmosphere, with largely unknown consequences for the Earth-climate system (Engel et al., 2017). A comprehensive understanding of the photochemical processes occurring at the SML and subsequent product formation in the gas phase and in the bulk aqueous phase is essential to improve our knowledge toward resolving the interactions within the sea-atmosphere interface (Gómez Alvarez et al., 2012). Compared to the subsurface water, the SML is often enriched with organic and inorganic compounds which persist at wind speeds of up to 10 m s^{-1}, without any observed depletion above 5 m s^{-1} (Wurl et al., 2011).

Although large efforts have been made to reduce the emission of polycyclic aromatic hydrocarbons (PAHs), their concentrations within the aquatic environment remain high (Keyte et al., 2013; Ravindra et al., 2008). These compounds are ubiquitous in the SML, emerging from various sources such as gasoline and diesel vehicles, refuse incineration, and coal-fired power stations (Hsu et al., 2016). The primary emitted PAHs are deposited into the surface waters via atmospheric deposition (Ma et al., 2013). It has been shown that the air-water diffusive exchange is the main source of two to five ring PAHs at the ocean surface (González-Gaya et al., 2019). The concentrations of PAHs in sea surface water were reported to range from 5 to 1,930 ng L^{-1} (Ma et al., 2013; Otto et al., 2015; Pérez-Cerrera et al., 2007; Valavanidis et al., 2008). The

PAHs concentrations in particulate phase at the ocean surface are ranging from 2 up to 40 ng m^{-3} (González-Gaya et al., 2016). A number of PAHs have been also detected in fog waters at concentrations in the order of μg L^{-1} (Ehrenhauser et al., 2012; Franz et al., 2012).

The accumulation of PAHs at the water interface leads to enhanced surface concentration of PAHs (Chen et al., 2006; Cincinelli et al., 2001; Lohmann et al., 2009; Seidel et al., 2017). For example, in the Gulf of Mexico Seawater the concentrations of PAHs were about 8 times higher in the surface water (0–1 m) compared to deep water (10–200 m) (Boehm et al., 2016). Indeed, theoretical calculations performed at a molecular level indicate that the interfacial region provides an energetic sink for the enrichment of PAHs (Vacha et al., 2006; Veljković, 2018). The interfacial region, although only a few Angstroms thin, plays an important role for the enhanced photodegradation of PAHs at the SML compared to the bulk, as the highest concentrations of PAHs (Carpenter & Nightingale, 2015; Liss & Duce, 1997), as well as the highest intensity of Ultraviolet–visible (UV-VIS) light that occurs at the SML (Li et al., 2015; Vasilkov et al., 2001).

Fluorene (FL), as a three-ring aromatic hydrocarbon, is known to be one of the most abundant PAHs enriched at the SML (Cincinelli et al., 2001; Hardy et al., 1990). It is also one of the U.S. Environmental Protection Agency's and the European Union's priority because it has water solubility significantly higher than the other PAHs, especially those with higher molecular weights (Kinani et al., 2016).

Dimethyl sulfoxide (DMSO) represents the most abundant organic sulfur (OS) compound in the oceans arising from the photooxidation and bacterial transformation of dimethyl sulfide (Barnes et al., 2006; Hoffmann et al., 2016; Simo & Vila-Costa, 2006). The exchange with the atmosphere is an additional source of DMSO to the sea surface. Because of the high Henry's law coefficient in the order of 10^7 M atm^{-1}, it is expected the net exchange directed from the atmosphere to the sea water (Legrand et al., 2011). Decades of research on the (photo)oxidation processes of PAHs have provided fundamental and practical insights into these processes especially in the gas phase (Keyte et al., 2013; Zelenyuk et al., 2017; Zhou et al., 2019). Only more recently, however, the oxidation of PAHs has been investigated in atmospheric heterogeneous environments (e.g., Donaldson et al., 2009; Monge et al., 2010; Styler et al., 2011; Zhou et al., 2019). It is known that the photodegradation of some PAHs is significantly slower in organic solvents than in aqueous solution (Grossman et al., 2016). However, the structure and, importantly, the pathways of formation for many organic compounds formed photochemically still remain unclear. To the best of our knowledge, there is only one study in the literature reporting the photoproducts of FL in the aqueous phase (Kinani et al., 2016). The model estimations indicate that photochemical processes occurring at the air-sea interface serve as an important source of volatile organic compounds and organic aerosol mass loadings, able to compete with primary emitted particles from biological processes occurring in the ocean (Brüggemann et al., 2018). Thus, within the present study the formation of gas phase products was assessed by the assistance of single photon ionization time of flight mass spectrometry and secondary electrospray ionization (SESI) high-resolution mass spectrometry. The condensed phase products formed during the light-induced degradation of FL/DMSO mixtures were evaluated by the means of ultrahigh resolution electrospray ionization Fourier-transform ion cyclotron resonance mass spectrometry (FT-ICR-MS). Based on the broad and complex spectrum of organic products formed in the aqueous and gas phases, the thermodynamic feasibility of the proposed detailed reaction schemes was examined by quantum mechanical calculations using density functional theory. Transient spectroscopy with a laser flash photolysis was used to assess the excited triplet state of fluorene ($^3FL^*$) and its reactivity toward DMSO.

2. Methodology and Instruments

2.1. Experimental Setup

A double-wall rectangular photoreactor was made up of borosilicate glass, with dimensions 5 × 5 × 2 cm. The photoreactor was thermostated at 20 °C by thermostatic bath (LAUDA ECO RE 630 GECO, Germany).

In order to solubilize FL (1×10^{-4} mol L^{-1}) (Sigma-Aldrich, 98%), a mixture of DMSO and water (10:90 v/v) corresponding to a DMSO concentration of 1.4 mol L^{-1} was used as solvent. We have chosen DMSO not only because it can help dissolve FL but also because it is an abundant organic compound at the sea surface. Such high concentrations of the solvent were used before to study the effect of solvent on PAHs photolysis (Grossman et al., 2016). It was shown that organic solvents may affect PAH reactivity by changing the local environment (Donaldson et al., 2009; Grossman et al., 2016; Librando et al., 2014). The reactor was filled

with 10 ml of freshly prepared solution (Figure S1 in the supporting information (SI)). The reactor was continuously flushed with 200 ml min^{-1} (range 0–500 ml min^{-1}, Sevenstar CS200 mass flow controller; accuracy, ±1%) of purified air, carrying the gas phase products to different analytical tools described below. This experimental setup was chosen to simulate conditions at the air-sea interface on calm water covered by an organic film (FL/DMSO) as a SML proxy. The organic film that consisted of FL/DMSO was visible to the naked eye. Considering that PAHs and DMSO are mostly concentrated at the water surface, we assume that the photochemical degradation of FL/DMSO occurs at the surface.

After 4 hr of irradiation, aliquots of 1 ml were taken from the photoreactor and directly injected into a FT-ICR-MS for the analysis of liquid phase products. The mass spectrometric analysis was performed immediately after sampling, thereby avoiding sample storage. In this context it is worth noting that recently, it has been shown that the sample fractionation prior to direct injection to FT-ICR-MS leads to much more detailed insights of molecular composition. Furthermore, losses during the separation method cannot be ruled out as some molecular formulae might be missing despite careful sample processing (Spranger et al., 2019).

Blank experiments were routinely performed using 18 MΩ deionized water and solutions containing FL/DMSO under dark conditions to determine the background signals.

A pH meter (ORION STAR A326, Thermo Scientific, USA) was used to measure the pH value of the FL/DMSO solution, which was determined to be 5.72 ± 0.03 before irradiation and 7.47 ± 0.05, after 4 hr of irradiation, respectively. All experiments were performed in duplicate.

2.2. Irradiation Procedure

The solution was irradiated for up to 4 hr by solar simulator (Xe-lamp) positioned at a 10 cm distance from the reactor simulating solar irradiation conditions. A water filter was applied to remove infrared radiation, in addition to a cutoff filter allowing radiation in the wavelength range of 300 nm ≤ λ ≤ 700 nm to pass, similar to the conditions at the lower layer of the atmosphere, close to the Earth surface. To characterize the photoreactor, the emission spectrum was measured in an empty reactor with a calibrated spectroradiometer (Ocean Optics, USA) equipped with a linear array CCD detector. The actinic flux was determined from the measured spectral irradiance and compared with the solar actinic flux (Figure S2). The total actinic fluxes integrated in the range of wavelengths between 300 and 400 nm of the sunlight and solar simulator were, respectively, 4.4×10^{15} and 5.9×10^{15} photons cm^{-2} s^{-1}. The emitted photon flux by the solar simulator is close to the solar actinic flux in the ultraviolet wavelength range.

2.3. Instrumentation

2.3.1. FT-ICR-MS

The formation of products in the bulk aqueous phase was analyzed with a solariX XR FT-ICR MS instrument (Bruker Daltonik GmbH, Bremen, Germany) equipped with a refrigerated, 9.4 T actively shielded superconducting magnet (Bruker Biospin, Wissembourg, France) and a Paracell analyzer cell. The ionization of the samples was performed in the negative ion mode using an ESI ion source (Bruker Daltonik GmbH, Bremen, Germany). The detection mass range was set to *m/z* 150–1,000. Ion accumulation time was set to 0.65 s. A total of 64 continuous 4 M FT-ICR transients was co-added to enhance the signal-to-noise ratio and dynamic range. The mass spectra were calibrated externally with arginine clusters in the negative ion mode, using a linear calibration. The final spectrum was internally recalibrated with typical O_2 class species peaks using quadratic calibration in DataAnalysis 4.4 (Bruker Daltonics). A typical mass-resolving power (m/Δm50%, in which Δm50% is the magnitude of the mass spectral peak full width at half-maximum peak height) >450,000 was achieved at *m/z* 319, with <0.3 ppm absolute mass error.

In-house software was used to calculate all mathematically possible formulas for all ions with a signal-to-noise ratio above 10, using a mass tolerance of ±1 ppm. The maximum number of atoms for the formula calculator was set to 30 ^{12}C, 60 ^{1}H, 20 ^{16}O, 3 ^{14}N, 1 ^{32}S, 1 ^{13}C, 1 ^{18}O, and 1 ^{34}S. For the chemical formula $C_cH_hO_oN_nS_s$, the double bond equivalent (DBE) is calculated using the following equation: DBE = (2c + 2 − h + n)/2. Detailed information about data processing is given in previous publications (Jiang et al., 2014; Jiang et al., 2016).

2.3.2. A Photon Ionization Time-of-Flight Single Mass Spectrometer

A photon ionization time-of-flight single mass spectrometer (SPIMS 3000, Guangzhou Hexin Instrument Co., Ltd., China) was employed to detect the gas phase products during the photosensitized reactions of

FL. A polydimethylsioxane (thickness 0.002 int, Technical Products Inc, USA) membrane was used in the injector of the TOF-MS. A vacuum ultraviolet light emitted by a deuterium (D2) lamp (Hamamatsu, Japan) was used for ionization of the organic compounds. Single photon ionization, with a 10.8 eV energy of single photons, is capable of a performance of the "soft" ionization of detected organics.

The ToF mass analyzer consists of a double-pulsed acceleration region, a field-free drift tube, a reflector, and an ion detector. The length of the double-pulsed acceleration region is 52 mm. The field-free drift region is 300 mm long and held at electric field potential of 2,200 V where the ions drift at a constant speed. The reflector is separated into two stages with different field strengths by grid at Earth electric potential. The first stage and second stage are 90 and 35 mm long, respectively. Two micro channel plates (MCP) assembled with chevron-type are used for the ion detector. A 350 MHz analog-to-digital converter was used for measuring and recording the output current signal from MCP. The limit of detection of TOF-MS is around 1 ppb for majority of the trace gases.

2.3.3. SESI High-Resolution Mass Spectrometry (The Orbitrap-MS)

Direct detection of formed volatile organic compounds was studied by employing another ultrahigh resolution Hybrid Quadrupole Orbitrap Mass Spectrometer (Orbitrap-MS) with its highest mass-resolving power of 1.4×10^5 and a mass accuracy of $\leq$2 ppm (Zeng et al., 2020). For the real-time analysis of the gas phase products the Orbitrap-MS was interfaced with a homemade SESI source. The modification of SESI source from a commercial nano-ESI was established by the connection of a compact stainless steel ionization chamber to the curtain plate of the MS vacuum interface. The operated Orbitrap-MS coupled with SESI has the ability to sensitively distinguish low-intensity isobaric features and to accurately identify the elemental compositions of unknown gas phase compounds. A homemade Sec-nanoESI source chamber was hyphenated to a commercial Orbitrap-MS (Thermo Scienfitic, USA). Gas phase samples were directly brought into the stainless steel SESI chamber through a 4 mm I.D. Teflon tube. The flow of gas phase samples was crossed with the nano-ESI plume and subsequently ionized. Ultrapure water with a resistance of 18.2 MΩ cm^{-1} was operated as ESI solvent. The flow rate of ESI solvent was adjusted at 200 nl min^{-1} and stably supplied with a nano-LC system (Thermo Scientific, USA). The temperature of the ion transfer capillary was held at 150 °C. The MS analyses were operated in the mass range between m/z 50 and 500. The samples were scanned in both positive and negative ion detection modes, and the ESI voltage was established to 2.5 and −2.5 kV, respectively. The Orbitrap-MS was calibrated with commercial standard calibration solutions (Thermo Scientific, USA) before measurements.

2.3.4. Laser Flash Photolysis

Triplet state detection and reactivity have been investigated using transient spectroscopy with a laser flash photolysis (LFP) apparatus as described before (Brigante et al., 2010). The fourth harmonic (λ_{exc} = 266 nm) of a Nd:YAG laser is used for the excitation of DMSO/water solutions of FL with an energy of 50 mJ per pulse. An appropriate volume of FL stock solution in DMSO was diluted or mixed with water just before each experiment to obtain the desired mixtures and concentration. The corresponding ultraviolet spectra of FL at different conditions are depicted in Figure S3. A peristaltic pump was used to continuously replace the solution inside the quartz cell to avoid sample degradation after the LFP pulse and analysis. All experiments were performed at ambient temperature (293 ± 2 K) and in aerated solutions (unless stated otherwise). A monoexponential decay equation was used to fit the absorption versus time plot to obtain the pseudo first-order constant (k', s^{-1}). The second-order constant (k, M^{-1} s^{-1}) for the quenching with DMSO and oxygen was determined from the linear fit of k' as function of quencher concentration. The error bars are determined as $\pm 3\sigma$, obtained from the scattering of the experimental data from the fitting line.

2.4. Theoretical Calculations

The geometries of all molecules involved in the oxidative degradation schemes were optimized, and their vibrational frequencies were derived at the PM7 level of theory, (Stewart, 2013) using the MOPAC program (Stewart, 2016). A detailed description of the computational procedure is presented in SI. The calculated PM7 geometries of all species are presented in Table S1. The B3LYP-CPCM/aug-cc-pVTZ energetics of the dominant configurations are presented in Tables S2 and S3, and the corresponding reaction Gibbs energies at 298.15 K are shown in Schemes 1 and 2, in the aqueous and in the gas phase, respectively (*vide infra*).

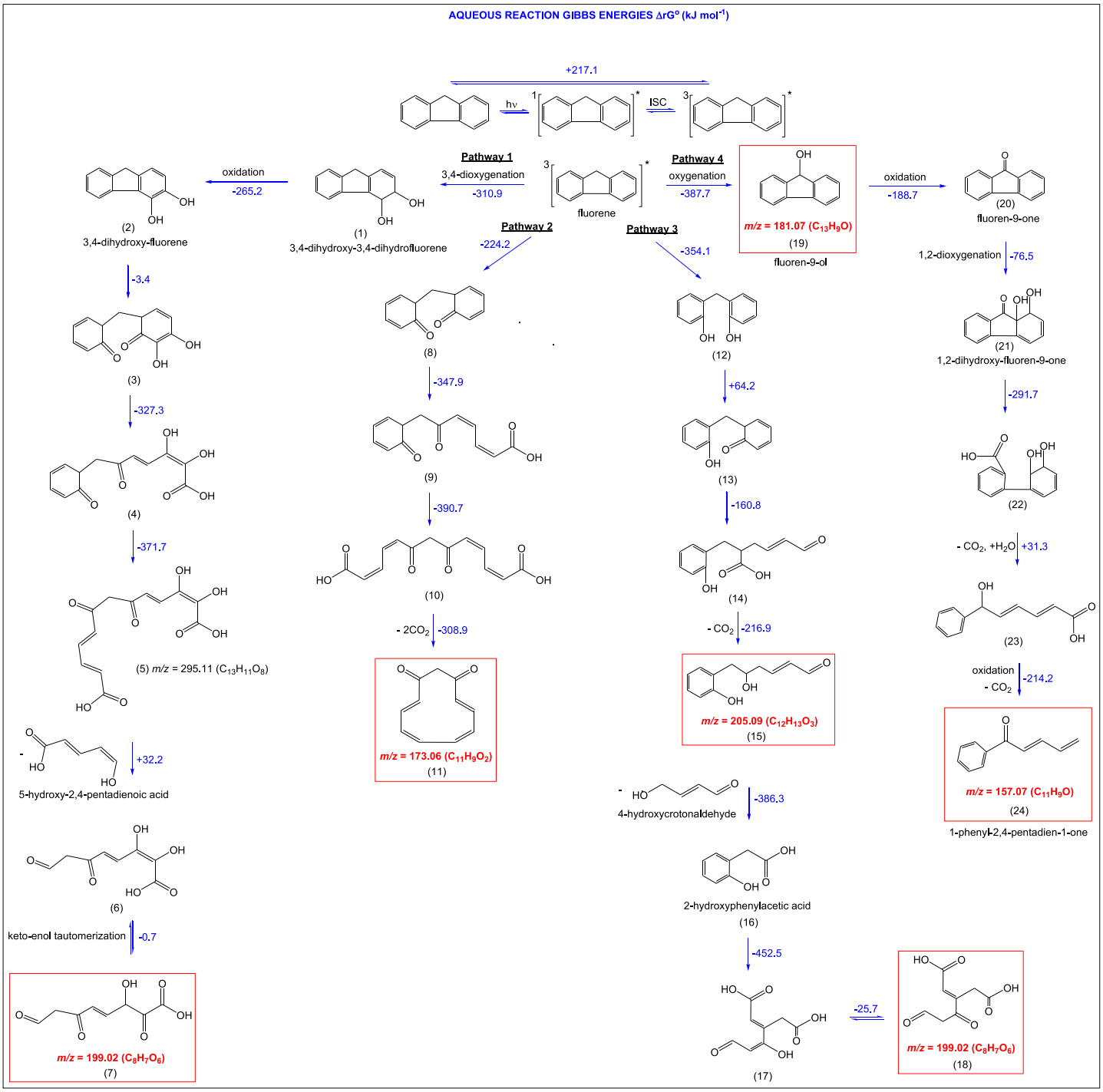

Scheme 1. Detailed reaction mechanism describing the formation of aqueous phase products initiated by ^{3}FL*. Numbers in brackets, written below each molecule, present compound designations to follow the discussion better with the Scheme 1. All identified products are framed into red rectangles.

3. Results and Discussion

3.1. Kinetics

Transient spectra obtained from a 266-nm excitation of 1×10^{-4} mol L^{-1} of FL in DSMO and DMSO/H_2O 1/9 solutions are reported in Figures S4a and S4b. In the DMSO/H_2O solution the main peak of the transient spectrum of FL (see the SI) is centered at 370 nm exhibiting a first-order rate

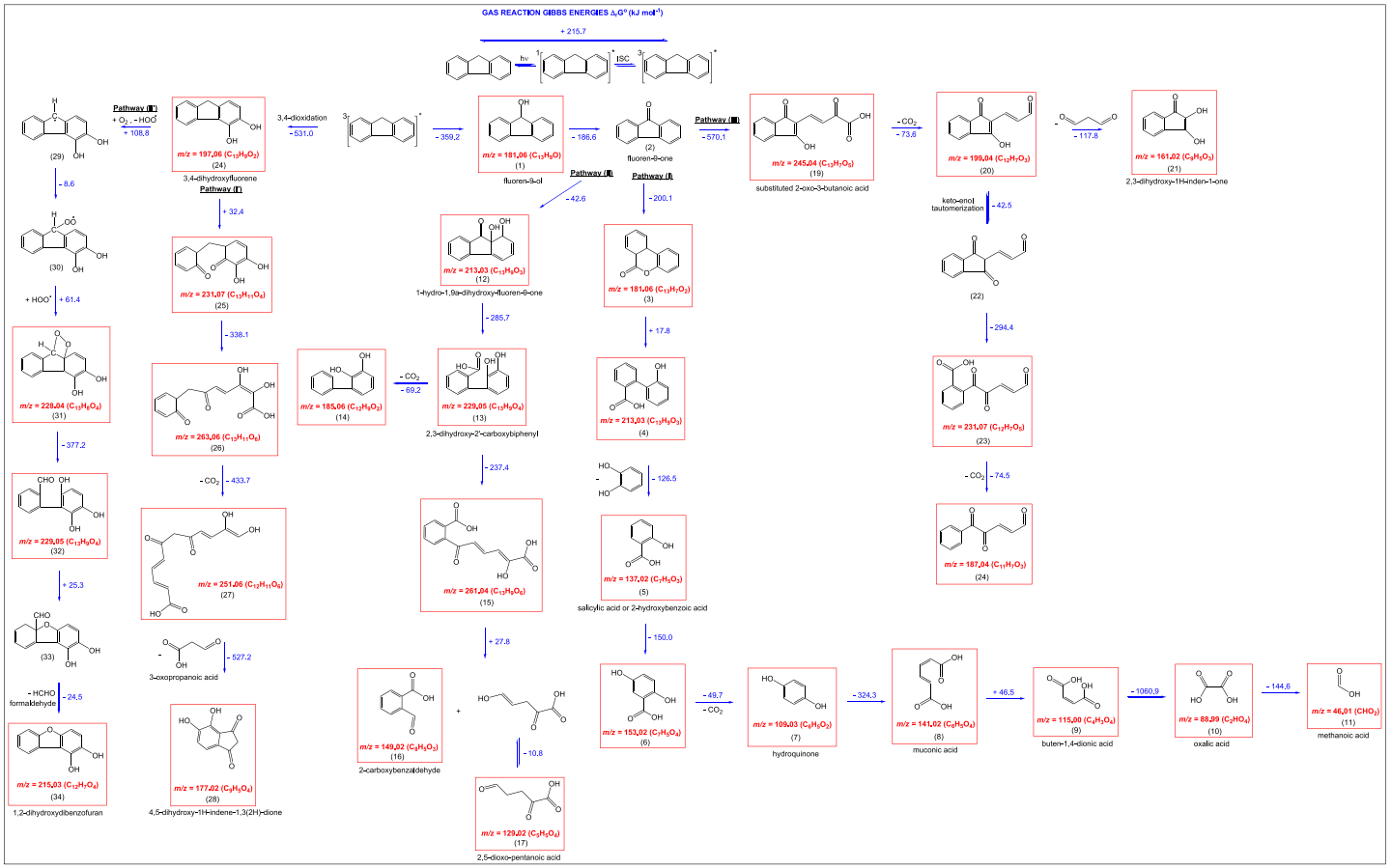

Scheme 2. Detailed reaction mechanism describing the formation of gas phase products initiated by ^{3}FL*. Numbers in brackets, written below each molecule, present compound designations to follow the discussion better with the Scheme 2. All identified products are framed into red rectangles

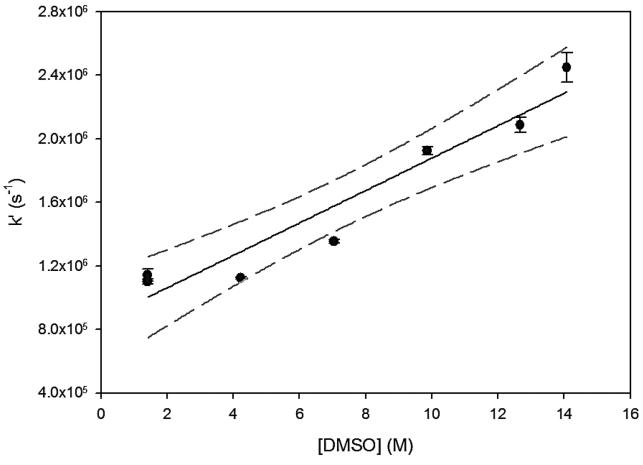

Figure 1. Pseudo first-order quenching rate constant of ^{3}FL* monitored at 370 nm, produced upon 266 nm excitation as a function of DMSO concentration in water. Error bars derived at the 3σ level determined from the scattering of the data fitting. Regression line (dashed) represents the 95% confidence bands.

constant $k_{1st} = (1.1 \pm 0.04) \times 10^6$ s^{-1}. To demonstrate that the signal observed at 370 nm corresponds to the triplet state of FL, the quenching in DMSO solution was investigated under aerated, oxygen, and argon saturated solutions (Figure S5). The linear correlation between the decay of ^{3}FL* monitored at 370 nm and O_2 concentration (inset of Figure S4) gives a second-order rate constant k_{FL^*,O_2} $k_{2nd} = (8.6 \pm 0.2) \times 10^9$ M^{-1} s^{-1} indicating that the effective quenching of ^{3}FL* corresponds to formation of singlet oxygen ($^1O_2$) in solution (Gorman & Rodgers, 1989) as reported for other PAHs in water (Brigante et al., 2010). It has been shown that $^1O_2$ is formed by energy transfer upon excitation of many PAHs (DeRosa & Crutchley, 2002), including FL (Barbas et al., 1996; Han et al., 2012). Indeed, quantum mechanical calculations using density functional theory at the B3LYP-CPCM/aug-cc-pVTZ level indicate the presence of a triplet state lying at 215.7 kJ mol^{-1} above the ground state. The reactivity between ^{3}FL* and DMSO was determined following the decay of the signal at 370 nm as a function of DMSO concentration in water (Figure 1). The linear fit of k_{1st} versus DMSO concentration gives a rate constant of $(1.0 \pm 0.1) \times 10^5$ M^{-1} s^{-1}. These data clearly demonstrate that DMSO can react with the triplet state of FL.

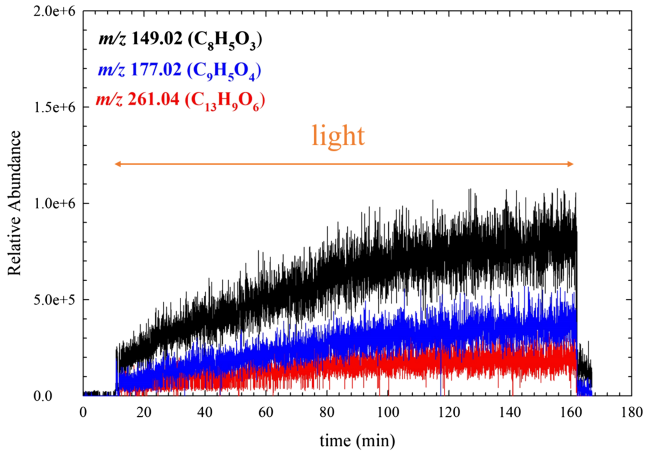

Figure 2. The time evolution of selected ions recorded by SESI-HRMS.

3.2. Direct Gas Phase Products Measurements With SESI-Orbitrap-High-Resolution Mass Spectrometry

We show that under sunlight irradiation, the excited triplet state of FL ($^3FL^*$), used here as a proxy for more PAHs present in the SML (Barbas et al., 1996; Barbas et al., 1997; Fasnacht & Blough, 2002; Fasnacht & Blough, 2003), releases a broad variety of saturated and unsaturated oxygenated multifunctional compounds (e.g., m/z 261.04 ($C_{13}H_9O_6$) in the gas phase (Figure 2), through a photosensitized process. Figure 2 shows typical profiles of gas phase products formed immediately upon irradiation of FL and DMSO.

Upon light irradiation of FL/DMSO, a prompt formation of a C8 aldehyde (m/z 149.02 ($C_8H_5O_3$)) was observed in the gas phase, which is most probably 2-carboxybenzaldehyde, (Figure 2 and Scheme 2). This aldehyde is a highly toxic compound even at very low concentrations (Sepic et al., 2003). The formation of another toxic compound, m/z 215.03 ($C_{12}H_7O_4$) (1,2-dihydroxydibenzofuran) was also detected. Indeed, many of the gas phase products, which are tentatively assigned to, for example, fluoren-9-ol and fluoren-9-one (Scheme 2), are found to be more toxic than FL (Sepic et al., 2003). The prompt formation of highly oxygenated multifunctional unsaturated compounds (e.g., m/z 261.04 ($C_{13}H_9O_6$) and highly oxygenated aromatic compounds (e.g., (e.g. m/z 177.02 ($C_9H_5O_4$)) was also detected. From the previous studies (Dabrowska et al., 2005; Kinani et al., 2016), we can reasonably assume that these primary gas phase compounds have a high probability to be formed during the photodegradation of FL.

As soon as the light source was turned off, a prompt decrease of the signals to the background levels was observed (Figure 2).

3.3. Analysis of FT-ICR-MS Aqueous Phase Products

The results obtained by using FT-ICR-MS revealed that the molecular composition of the liquid phase products formed upon 4 hr of FL/DMSO irradiation was very complex, exhibiting a wide mass distribution of the reaction products.

The iso-abundance plot of DBE versus carbon numbers for the detected $C_cH_hO_o$ compounds formed upon photosensitized chemistry initiated by FL is presented in Figure 3. DBE is the number of double bonds plus rings present in the organic compounds.

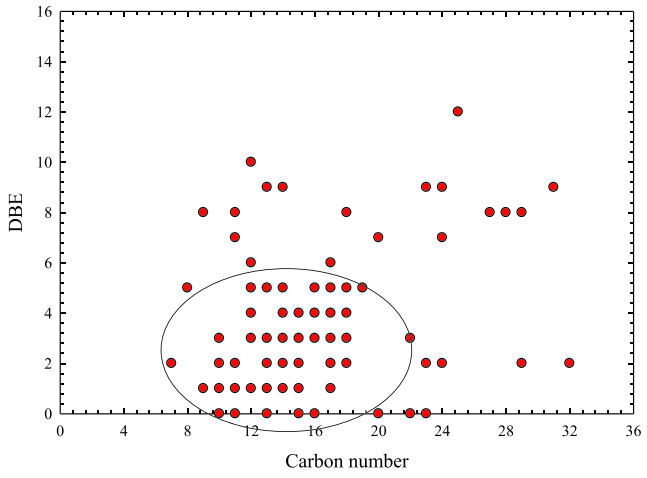

Figure 3. DBE versus carbon number isoabundance plot for the $C_cH_hO_o$ group of compounds, emerged upon 4 hr of irradiation of FL.

Most of the $C_cH_hO_o$ liquid phase products formed upon photosensitized interfacial chemistry of FL exhibit DBE values in the range between 2 and 6, with 7 to 20 carbon atoms and 5 to 8 oxygen atoms (circled in Figure 3). These high molecular weight organic compounds contain two to six carbonyl groups with several oxygen-containing moieties like hydroxyl or carboxyl, depending on the occurrence of different oxygen atoms (Mekic et al., 2018; Mekic et al., 2019; Vione et al., 2019). The $C_cH_hO_o$ with the same DBE values but different carbon numbers are considered as homologs differing from each other by a repeating mass increment (Jiang et al., 2014).

By implementing the VK diagram, the compositional characteristics of complex organic mixtures could be displayed, as this kind of plot gives a broad overview on the average properties in terms of H/C and O/C ratios of its molecules (Kim et al., 2003; Lin et al., 2012; Rincon et al., 2012; Wang et al., 2017; Wang et al., 2018; Wu et al., 2004) The two-dimensional VK plot for all $C_cH_hO_o$ compounds, observed in ESI^- with *m/z* between 150 and 700 is shown in Figure 4. Based on the values of H/C and O/C ratios, organic compounds could be separated into two different groups. The compounds presented in Region A, which exhibit

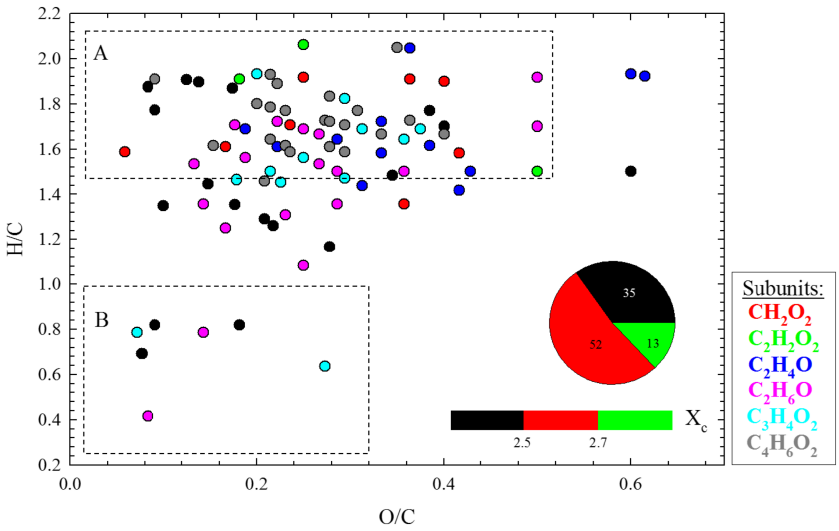

Figure 4. The van Krevelen graph for $C_cH_hO_o$ group of compounds, formed upon 4 hr of light irradiation of FL/DMSO and detected in ESI^- mode. The recognized repeating mass building increments are labeled in the legend. All other molecules which do not participate in any building block increments are depicted in black color. A and B areas depict oxygenated aliphatic compounds and low-oxygenated aromatic hydrocarbons, respectively. The aromaticity equivalent (black with $X_c < 2.5$, red with $2.5 \leq X_c < 2.7$, and green with $X_c \geq 2.7$) is illustrated by the color bar, while the pie chart demonstrates the percentage value of each color-coded compound in the sample.

high H/C ratios (≥1.5) and low O/C ratios (≤0.5), could correspond to oxygenated aliphatic compounds, containing at least two oxygen atoms in each formula. In contrast, the compounds displayed in the lower left corner of the diagram (Region B), characterized by low H/C (≤1.0) and O/C (≤0.5) ratios may correspond to low oxygen-containing aromatic hydrocarbons (Lin et al., 2012). The low H/C and O/C ratios suggest the formation of unsaturated characteristics of $C_cH_hO_o$ compounds, which is further approved by the aromaticity equivalent (X_c), a parameter for the identification and characterization of aromatics ($X_c \geq 2.5$) and condensed aromatics ($X_c \geq 2.7$), as described in detail by Yassine et al. (2014). As shown in the pie chart of Figure 4, about half of the formed products contain aromatic structure in a molecule; meanwhile, 35% of all $C_cH_hO_o$ compounds might appear as aliphatic compounds after 4 hr of photolysis. The remaining 13% are condensed aromatic compounds.

Based on the van Krevelen plot, the regular addition of the repeating mass building increments within all the identified series is responsible for the increase in the molecular mass of the detected compounds (Altieri et al., 2006; Mekic et al., 2018). Further details about the van Krevelen presentation of the experimental data and the formation of high-molecular weight compounds are given in the supporting information (Figures S6 and S7).

3.4. Reaction Mechanisms

The initial step of photochemical mechanism is the photoexcitation of FL through the $\pi \rightarrow \pi^*$ electronic transition, followed by intersystem crossing to produce the excited triplet state ($^3FL^*$). $^3FL^*$ can react following different pathways in water/DMSO solution: (i) through energy transfer reaction with triplet state oxygen ($^3O_2$) leading to the formation of singlet oxygen ($^1O_2$). $^1O_2$ can react with FL (on the electron rich double bonds) with a rate constant of ~10^5 M^{-1} s^{-1} (Wilkinson et al., 1995) presumably forming dioxetanes derivative products followed by formation of aldehydes/ketones. (ii) *Via* reactivity with water as recently observed for other triplets states (Brigante et al., 2010) leading to the formation of hydroxyl radical (via water oxidation). Hydroxyl radical (OH) can oxidize FL or its degradation products (iii) reacting with DMSO through electron transfer leading to the formation of radicals. The information obtained from the detected products in the gas phase and in the bulk water was used to develop a detailed scheme of reaction pathways for the photosensitized degradation of FL, depicted in Schemes 1 and 2. These comprehensive reaction schemes fully explain the majority of the detected unsaturated multifunctional compounds emerging from the photosensitized processing of FL and DMSO at the air-water interface.

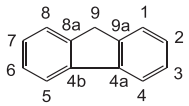

Figure 5. FL and its numbering convention.

The quantum mechanical calculations (described fully in the SI) indicate that all suggested reaction channels are energetically feasible.

3.4.1. Reaction Mechanisms in the Aqueous Phase

Based on the distribution of the identified reaction products in the liquid phase, four possible reactions initiated by $^3FL^*$ are proposed which are complementary to the reaction mechanism suggested by Kinani et al. (2016). In the following section the numbers in parenthesis represent the detected products which are depicted in the reaction Schemes 1 and 2. Pathway 1 describes the reaction between $^3FL^*$, and O_2 yields 3,4-dihydroxy-3,4-dihydrofluorene (1), ($\Delta_rG^0 = -310.9$ kJ mol^{-1}) which is further transformed by oxidation to 3,4-dihydroxy-fluorene (2).

The degradation of latter compound (2) could involve the O_2 attack of the saturated five-membered ring at 4a/4b position (Figure 5), allowing the ring to open (3) (Scheme 1).

Once the five-membered ring is activated (3), further degradation is centered at the aromatic ring, initiating the cleavage of the aromatic body at the 4a/9a position of $^3FL^*$ (4). Furthermore, the opening of phenyl ring at the 4a/9a position of FL (4), followed by another phenyl ring opening at the position 4b/8a, could yield acyclic structure (5) with chemical composition $C_{13}H_{11}O_8$ (−371.7 kJ mol^{-1}). By the cleavage of 5-hydroxy-2,4-pentadienoic acid from the acyclic structure (5), a highly oxidized unsaturated compound (7) could be formed via tautomeric rearrangement (−0.7 kJ mol^{-1}).

Pathway 2: Similarly to the activated five-membered ring (8) triggers phenyl ring opening (first at the 4a/9a (9) and second at the 8a/4b position of $^3FL^*$ (10), (Figure 5)) which after decarboxylation leads to the formation of a cyclic structure (11) (−308.9 kJ mol^{-1}). Likewise, reaction of $^3FL^*$ with O_2 affords scission of a five-membered ring at the 4a/9a position (Figure 5), yielding bisphenolic product (12) as illustrated in Pathway 3. After oxidation of only one phenolic group into cyclohexadienoic form (13), the opening of the letter phenyl ring (14) was accompanied by decarboxylation, giving arise to $C_{12}H_{13}O_3$ (15) (−216.9 kJ mol^{-1}). The identified product is further transformed through the cleavage of 4-hydroxycrotonaldehyde to 2-hydroxyphenylacetic acid (16). Subsequently, the opening of the phenyl ring (substantially exoergic −452.5 kJ mol^{-1}) might cause the formation of a highly oxidized unsaturated compound (18) (m/z = 199.02) via keto-enol tautomerization (17) (−25.7 kJ mol^{-1}).

The fourth suggested pathway begins with an initial oxidation of $^3FL^*$ which occurs at the 9-position (Figure 5) due to the enhanced reactivity of the hydrogen atoms at this position, ascribed to the high acidity of FL (Tubaro et al., 2003). The formation of fluorene-9-one (20) proceeds plausibly by oxidation of fluoren-9-ol (19) (m/z = 181.07) formed during the initial mono-oxidation of $^3FL^*$. Fluorene-9-one is expected to undergo additional oxidation, resulting in a substituted biphenyl molecule (21). Moreover, oxygen attack initiates opening of the five-membered ring at position 9/9a (22) and by the following processes of decarboxylation and oxidation 1-phenyl-2,5-pentadien-1-one (24) (−214.2 kJ mol^{-1}) might be afforded.

3.4.2. Reaction Mechanisms for the Formation of the Gas Phase Products

Similarly, a multitude of compounds were detected in the gas phase, as a result of five different photodegradation pathways. In fact, three (I–III) of the proposed degradation mechanisms are initiated by fluorene-9-one (2), which is formed after mono-oxidation of methylene bridge in $^3FL^*$, similar to already explained mechanism in the aqueous phase. Pathway (I): fluorene-9-one (2) through oxidation might afford a ring expanded lactone (3) (−200.1 kJ mol^{-1}), which under a rapid oxidative scission yields biphenyl compound with a chemical composition of $C_{13}H_9O_3$ (4) (+17.8 kJ mol^{-1}). The substituted biphenyl is subsequently transformed into salicylic acid (5) (−126.5 kJ mol^{-1}), which after photooxidation (6) (−150.0 kJ mol^{-1}) and decarboxylation (−49.7 kJ mol^{-1}) may be converted into hydroquinone (7) (Scheme 2). It is possible that ring cleavage of hydroquinone releases a substantial amount of energy (−324.3 kJ mol^{-1}) forming muconic acid (8), which undergoes deacetylation (+46.5 kJ mol^{-1}) to yield buten-1,4-dionic acid (9). Additionally, photooxidation of buten-1,4-dionic acid yields oxalic acid (10), through a highly exoergic process (−1060.9 kJ mol^{-1}), followed by its decomposition to methanoic acid (11) (−144.6 kJ mol^{-1}). Pathway (II): Similarly, the photooxidation of fluorene-9-one might lead to formation of 1-hydro-1,9a-dihydroxy-9-fluorene (12). Subsequently, oxygen attack initiates exoergic (−285.7 kJ mol^{-1}) opening of a five-membered ring at the 9/9a position (Figure 5) and results in 2,3-dihydroxy-2′-carboxybiphenyl (13). In addition, the formed biphenyl compound may follow a decarboxylation pathway, generating a product

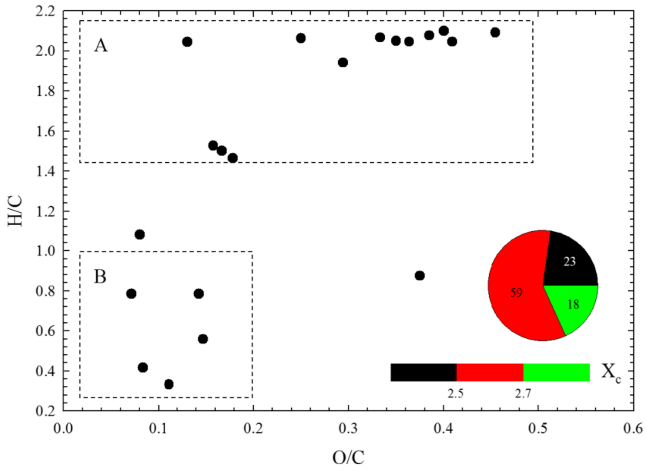

Figure 6. The van Krevelen graph for CHOS group of compounds, formed upon 4 hr of light irradiation of FL/DMSO and detected in ESI$^-$ mode. Areas "A" and "B" demonstrate oxygenated aliphatic compounds and low-oxygenated aromatic hydrocarbons, respectively. The aromaticity equivalent (black with $X_c < 2.5$, red with $2.5 \leq X_c < 2.7$, and green with $X_c \geq 2.7$) is depicted by the color bar, while the pie chart denotes the percentage value of each color-coded compound in the sample.

with a composition of $C_{12}H_9O_2$ (14) or continue with additional degradation. After the scission of five-membered ring, the degradation begins from the aromatic ring, which opens at the 4a/9a position (see Scheme S2 and Figure 5). It is possible that the cleavage of the aromatic ring leads to the formation of an oxidized and unsaturated compound with the *m/z* of 261.04 (15). Most probably, the nascent compound decomposes (+27.8 kJ mol^{-1}) via photooxidation into unsaturated, cyclic 2-carboxybenzaldehyde (16) and acyclic, highly oxidized 5-hydroxy-2-oxo-pent-4-enoic acid (17), respectively, which can be further converted via keto-enol tautomerization (−10.8 kJ mol^{-1}) to 2,5-dioxo-pentanoic acid (18). Pathway (III): fluorene-9-one could be also subjected to oxidative attack at carbon atoms C3 and C4 (Figure 5), followed by meta-cleavage in order to yield the substituted 2-oxo-3-butanoic acid (19) (−570.1 kJ mol^{-1}). Subsequently, the decarboxylation step (−73.6 kJ mol^{-1}) might generate a product with a chemical composition of $C_{12}H_7O_3$ (20), which can further proceed toward $C_3H_4O_2$ elimination (−117.8 kJ mol^{-1}), generating 2,3-dihydroxy-1H-inden-1-one (21) or toward keto-enol rearrangement (22) (−42.5 kJ mol^{-1}), accompanied by the cleavage of five-membered ring (23) (−294.4 kJ mol^{-1}) and followed by the decarboxylation (−74.5 kJ mol^{-1}) to generate a product with composition of $C_{11}H_7O_3$ (24).

^{3}FL* is expected to afford 3,4-dihydroxyfluorene (25) through oxygen attack. This reaction has previously been described and depicted in Scheme 1. There are two possible reaction pathways for 3,4-dihydroxyfluorene. Pathway (I'): additional oxygen attacks trigger all three substituted rings to open (26–28), as also occurring in the aqueous phase, accompanied by elimination of 3-oxopropanoic acid via a highly exoergic reaction (−527.2 kJ mol^{-1}) to generate 4,5-dihydroxy-1H-indene-1,3(2H)-dione (29). Pathway (II'): since FL has one sp^3 atom, the H-abstraction reaction (29) takes place readily at C9 (Figure 5) under the influence of delocalization energy yielding peroxy radical (30), which may proceed to creation of a four-membered ring (31). A scission of the four-membered ring is thermodynamically favored (−377.2 kJ mol^{-1}), yielding an intermediate (32) which subsequently undergo cyclization (33) with the formation of a potentially toxic product (−24.5 kJ mol^{-1}), 1,2-dihydroxydibenzofuran (34), after elimination of formaldehyde HCHO.

The used structures of all identified compounds in liquid phase and in the gas phase are based on the elemental compositions for a single mass, proposed by the used softwares (Compass DataAnalysis, Brucker for analysis of liquid-phase compounds and Thermo Xcalibur Qual Browser for determination of gas phase products), with low error (≤10 ppm). Hence, all the proposed structures should be regarded as tentative. In the future, the use of internal standards should reveal the structure of the detected compounds. In addition, theoretical calculations were performed to gain some insight into the transformation processes of ^{3}FL* in both liquid and gas phases.

3.4.3. Identification of OS Compounds

Figure 6 shows a VK diagram for the $C_cH_hO_oS_S$ compounds, emerged upon 4 hr irradiation of FL/DMSO. Similar to the $C_cH_hO_o$ compounds, the $C_cH_hO_oS_S$ subgroup is divided into two separated classes on the basis of the H/C and O/C ratios; Areas A and B. The compounds depicted in Region A with high H/C ratios (≥1.5) and O/C ratio below 0.5 might be linked with oxygenated aliphatic-like compounds. In contrast, the lower part of the CHOS-VK diagram (Region B) overlaps with the typical region of oxidized aromatic hydrocarbons as all the molecules in Area B exhibit low H/C (≤1.0) and O/C ratios (≤0.5) (see Figure 6) (Kourtchev et al., 2014). Moreover, the presence of aromatics could be additionally explained by the aromaticity equivalent (X_c), denoted in the form of the color bar (Figure 6). According to Yassine et al. (2014), a threshold X_c value, which usually serves as a criterion for identifying species with aromatic ring structures, should be in the range of $2.5 \leq X_c < 2.7$. Majority of the $C_cH_hO_oS_S$ compounds exhibit an aromatic structure in the molecules, regarding the red-colored fraction in the pie chart (Figure 6). However, the formed long-chain aliphatic-like $C_cH_hO_oS_S$ compounds still represent a significant fraction of the formed products, depicted with the black color in the pie chart, respectively.

Table 1
List of Compounds Found in Ambient Atmospheric Aerosols With the Same Molecular Compositions of S-Containing Products as Identified in the Present Study

m/z	Organosulfur products with formula $[M-H]^-$	Location of sampling	Period of sampling
191.034	$C_7H_{11}O_4S$	Guangzhou	winter
231.066	$C_{10}H_{15}O_4S$	Wuhan	winter
245.045	$C_{10}H_{13}O_5S$	Guangzhou, Wuhan	winter
247.061	$C_{10}H_{15}O_5S$	Guangzhou, Hong Kong, Wuhan, Nanjing, Shanghai	winter, summer, nighttime, daytime
223.028	$C_7H_{11}O_6S$	Guangzhou, Hong Kong, Wuhan, Nanjing, Shanghai	winter, summer, nighttime, daytime
237.117	$C_{10}H_{21}O_4S^*$	Guangzhou, Hong Kong, Wuhan, Nanjing, Shanghai	winter, summer, nighttime, daytime
267.111	$C_{11}H_{23}O_5S^*$	Wuhan	summer
295.158	$C_{13}H_{27}O_5S^*$	Wuhan	summer
321.211	$C_{16}H_{33}O_4S^*$	Wuhan, Nanjing, Shanghai	winter, summer, nighttime, daytime
323.19	$C_{15}H_{31}O_5S^*$	Wuhan	summer
349.205	$C_{17}H_{33}O_5S^*$	Wuhan, Shanghai	summer, daytime

Note. Light yellow color illustrates products found in the gas phase, whereas light blue color depicts products detected in bulk aqueous phase.
[a]Formation of alkyl-containing OS.

In this study, 22 $C_cH_hO_oS_S$ formulas were determined in ESI^- mode, found in the range between *m/z* 159 and 539. Moreover, the average molecular weight of the $C_cH_hO_oS_S$ molecules is much higher in comparison with $C_cH_hO_o$ compounds due to the presence of an additional sulfur (+32 amu) in the molecular structure. All of the S-containing organic compounds exhibit only one S-atom in their elemental composition. About 55% of the identified $C_cH_hO_oS_S$ formulae possess a molecular composition with $O/S \geq 4$, indicating presence of organosulfates. (Tao et al., 2014; Wang et al., 2016; Wang et al., 2018). However, the rest of the $C_cH_hO_oS_S$ compounds are assigned to exhibit distinctive hydrophobic characteristics (long aliphatic carbon chain) and unsaturation (DBE = 0), which could be summarized with elemental formula of $C_nH_{2n+2}O_{3\text{-}9}S^-$, where n is less or equal to 22. This highly abundant group of $C_cH_hO_oS_S$ compounds has already been detected in ambient rainwaters, aerosols, and PM2.5 samples (Altieri et al., 2009; Jiang et al., 2016; Lin et al., 2012; Tao et al., 2014). It was assumed that these OS species contain sulfur atom attached to carbon, which does not have any oxygenated functional groups on a long chain. Moreover, these S-containing organic compounds might be assigned not only as organosulfates (R-C-O-SO_3) but also as a newly discovered, aliphatic-like class of OS, where the term "aliphatic" takes into account CHOS species, having $C > 8$, DBE < 3, and $3 < O < 7$ (Tao et al., 2014; Lin et al., 2012; Wang et al., 2016; Kuang et al., 2016).

3.4.4. Comparison of OS Compounds Identified With Field Evidence

Some of the OS identified in this work exhibit elemental formulas consistent with S-containing compounds, identified in ambient samples at different locations in China (Guangzhou, Hong Kong, Wuhan, Nanjing, and Shanghai) highlighting the importance of the photosensitized reactions initiated by excited triplets of PAHs at the water surface (Kuang et al., 2016; Wang et al., 2016).

Table 1 shows the list of those compounds, the sampling location, and the period. It should be noted that accurate mass assignment, combined with MS^n (tandem mass spectrometry) experiments, is crucial for distinguishing multiple structural and stereo isomers. However, it should be noted that agreement between chemical formulas does not necessarily mean agreement between structures as multiple structural isomers are possible for each formula (Nizkorodov et al., 2011).

The sulfur-containing organic compounds, which have already been observed in the marine boundary layer, are likely to form more surfactant films on the aerosols, and consequently, they could affect surface tension and hygroscopicity of the formed particles (Decesari et al., 2011; Tao et al., 2014). Up to now, the possible precursors of these kind long alkyl chain OS are assumed to be long-chain alkanes, emitted by heavy traffic (Tao et al., 2014). As DMSO, also known as a dimethyl sulfide oxidation product (Hoffmann et al., 2016), is the only sulfur source in our study, it could react with light-absorbing compounds, like PAHs, and form large amount of products, presented in both liquid phase and gas phase. Hence, the results presented here suggest an additional source of S-containing organic compounds, formed through light-induced process and carried by excited triplet state of FL as a photosensitizer.

4. Conclusions and Implications

In the present study, it was shown that FL can act as a photosensitizer at the sea surface when irradiated by sunlight and may initiate the photochemical formation of oxygenated and unsaturated toxic organic compounds in both aqueous and gas phases. In particular, mixtures of FL/DMSO may be photochemically transformed into a variety of oxygenated, aliphatic, and aromatic compounds.

The toxicity of PAHs may be enhanced by abiotic processes such as the photosensitized transformation of FL, which, by virtue of the extensive π-orbital systems of PAHs, can be a major factor in PAHs toxicity (Huang et al., 1993). The compounds produced by photochemically generated $^3FL^*$ in the bulk aqueous phase are biologically much more active than FL itself, exerting significant estrogenic and dioxin-like activity (Kinani et al., 2010).

The photosensitized chemistry investigated in detail in the present work could indicate the involvement of a triplet state common to all PAHs at the water surface, which is accessible after sunlight absorption in the wavelength region between 300 and 400 nm. Since PAHs are ubiquitous at marine water surfaces (Cincinelli et al., 2005; González-Gaya et al., 2019; Guigue et al., 2011; Lim et al., 2007; Liu & Dickhut, 1997; Lohmann et al., 2009; Manodori et al., 2006; Stortini et al., 2009), the photosensitized production of gas phase unsaturated and multifunctional compounds can, first, convert PAHs in the marine SML and underlying water into their functionalized oxidation products which could furthermore affect marine surface ocean chemistry.

Second, as both SML and underlying water are involved in the generation of marine particles, the resulting functionalized and oxidized species are expected to be transferred into freshly generated marine aerosol particles and thus constitute a fraction of the organic mass in marine particles which has often been identified especially in small particles (Hersey et al., 2009).

More importantly, the results presented here suggest that the ubiquitous FL and DMSO at the SML represent an alternative source of OS compounds during daytime. This source is initiated by excited triplet state of FL and potentially of other PAHs (phenanthrene and pyrene) (Barbas et al., 1996; Monge et al., 2010) enriched at the ocean surface.

The oxygenated long-chain aliphatics and the organosulfur (OS) compounds emerging from the photosensitized chemistry of PAHs and DMSO can participate in secondary organic aerosol formation which in turn can better explain field observations of new particle formation events which are occurring independently of the primary emitted particles from marine biological activity (O'Dowd et al., 2004).

The presence of sea salts (NaCl, NaBr, and NaI) can eventually influence the photochemical process of FL/DMSO at the sea surface (Grossman et al., 2016; Stirchak et al., 2019). Ongoing studies in our lab are focused on the influence of sea salts on photochemical degradation of FL/DMSO, and the results will be published elsewhere.

Acknowledgments

This study was financially supported by the National Natural Science Foundation of China (41773131 and 41977187) and Chinese Academy of Science, International Cooperation Grant (N°: 132744KYSB20190007). We are grateful to Guangdong Foundation for Program of Science and Technology Research, Grant: 2017B030314057. Y. G. L acknowledges the support of this work by the project MIS 5002567, implemented under the "Action for the Strategic Development on the Research and Technological Sector," funded by the Operational Programme "Competitiveness, Entrepreneurship and Innovation" (NSRF 2014-2020) and cofinanced by Greece and the European Union (European Regional Development Fund). Data presented in this article can be found online (https://data.mendeley.com/datasets/szfdwkrvn5/1) (DOI: 10.17632/szfdwkrvn5.1).We also appreciate 'Hexin Analytical Instrument Co., Ltd., China' for their generous offer to provide SPIMS 3000.

Reference

Altieri, K. E., Carlton, A. G., Lim, H. J., Turpin, B. J., & Seitzinger, S. P. (2006). Evidence for oligomer formation in clouds: Reaction of isoprene oxidation products. *Environmental Science and Technology*, *40*(16), 4956–4960. https://doi.org/10.1021/es052170n

Altieri, K. E., Turpin, B. J., & Seitzinger, S. P. (2009). Oligomers, organosulfates, and nitrooxy organosulfates in rainwater identified by ultra-high resolution electrospray ionization FT-ICR mass spectrometry. *Atmospheric Chemistry and Physics*, *9*, 2533–2542.

Barbas, J. T., Sigman, M. E., Arce, R., & Dabestani, R. (1997). Spectroscopy and photochemistry of fluorene at a silica gel/air interface. *Journal of Photochemistry and Photobiology A: Chemistry*, *109*, 229–236.

Barbas, J. T., Sigman, M. E., & Dabestani, R. (1996). Photochemical oxidation of phenanthrene sorbed on silica gel. *Environmental Science and Technology*, *30*, 1776–1780.

Barnes, I., Hjorth, J., & Mihalopoulos, N. (2006). Dimethyl sulfide and dimethyl sulfoxide and their oxidation in the atmosphere. *Chemical Reviews*, *106*, 940–975.

Boehm, P. D., Murray, K. J., & Cook, L. L. (2016). Distribution and attenuation of polycyclic aromatic hydrocarbons in Gulf of Mexico seawater from the deepwater horizon oil accident. *Environmental Science and Technology*, *50*(2), 584–592. https://doi.org/10.1021/acs.est.5b03616

Brigante, M., Charbouillot, T., Vione, D., & Mailhot, G. (2010). Photochemistry of 1-nitronaphthalene: A potential source of singlet oxygen and radical species in atmospheric waters. *Journal of Physical Chemistry A*, *114*, 2830–2836.

Brüggemann, M., Hayeck, N., & George, C. (2018). Interfacial photochemistry at the ocean surface is a global source of organic vapors and aerosols. *Nature Communications*, *9*, 1–8.

Carpenter, L. J., & Nightingale, P. D. (2015). Chemistry and release of gases from the surface ocean. *Chemical Reviews*, *115*(10), 4015–4034. https://doi.org/10.1021/cr5007123

Chen, J., Ehrenhauser, F. S., Valsaraj, K. T., & Wornat, M. J. (2006). Uptake and UV-photooxidation of gas-phase PAHs on the surface of atmospheric water films. 1. Naphthalene. *Journal of Physical Chemistry A*, *110*, 9161–9168.

Cincinelli, A., Stortini, A. M., Checchini, L., Martellini, T., Del Bubba, M., & Lepri, L. (2005). Enrichment of organic pollutants in the sea surface microlayer (SML) at Terra Nova Bay, Antarctica: Influence of SML on superficial snow composition. *Journal of Environmental Monitoring*, *7*(12), 1305–1312. https://doi.org/10.1039/b507321a

Cincinelli, A., Stortini, A. M., Perugini, M., Checcjini, L., & Lepri, L. (2001). Organic pollutants in sea-surface microlayer and aerosol in the coastal environment of Leghorn—(Tyrrhenian Sea). *Marine Chemistry*, *76*, 77–98.

Dabrowska, D., Kot-Wasik, A., & Namiesnik, J. (2005). Pathways and analytical tools in degradation studies of organic pollutants. *Critical Reviews in Analytical Chemistry*, *35*, 155–176.

Decesari, S., Finessi, E., Rinaldi, M., Paglione, M., Fuzzi, S., Stephanou, E. G., et al. (2011). Primary and secondary marine organic aerosols over the North Atlantic Ocean during the MAP experiment. *Journal of Geophysical Research*, *116*, D22210. https://doi.org/10.1029/2011JD016204

DeRosa, M. C., & Crutchley, R. J. (2002). Photosensitized singlet oxygen and its applications. *Coordination Chemistry Reviews*, *233-234*, 351–371.

Donaldson, D. J., & George, C. (2012). Sea-surface chemistry and its impact on the marine boundary layer. *Environmental Science and Technology*, *46*(19), 10385–10389. https://doi.org/10.1021/es301651m

Donaldson, D. J., Kahan, T. F., Kwamena, N.-O. A., Handley, S. R., & Barbier, C. (2009). In K. Valsaraj (Ed.), *Atmospheric chemistry of urban surface films* (pp. 79–89). American Chemical Society. https://doi.org/10.1021/bk-2009-1005.ch006

Ehrenhauser, F. S., Khadapkar, K., Wang, Y., Hutchings, J. W., Delhomme, O., Kommalapati, R. R., et al. (2012). Processing of atmospheric polycyclic aromatic hydrocarbons by fog in an urban environment. *Journal of Environmental Monitoring*, *14*(10), 2566–2579. https://doi.org/10.1039/c2em30336a

Engel, A., Bange, H. W., Cunliffe, M., Burrows, S. M., Friedrichs, G., Galgani, L., et al. (2017). The ocean's vital skin: Toward an integrated understanding of the sea surface microlayer. *Frontiers in Marine Science*, *4*, 1–14.

Fasnacht, M. P., & Blough, N. V. (2002). Aqueous photodegradation of polycyclic aromatic hydrocarbons. *Environmental Science and Technology*, *36*(20), 4364–4369. https://doi.org/10.1021/es025603k

Fasnacht, M. P., & Blough, N. V. (2003). Kinetic analysis of the photodegradation of polycyclic aromatic hydrocarbons in aqueous solution. *Aquatic Science*, *65*, 352–358.

Franz, S., Khadapkar, K., Wang, Y., Hutchings, J. W., Delhomme, O., Kommalapati, R. R., et al. (2012). Processing of atmospheric polycyclic aromatic hydrocarbons by fog in an urban environment. *Journal of Environmental Monitoring*, *14*, 2566–2579.

Gómez Alvarez, E., Wortham, H., Strekowski, R., Zetzsch, C., & Gligorovski, S. (2012). Atmospheric photo-sensitized heterogeneous and multiphase reactions: From outdoors to indoors. *Environmental Science and Technology*, *46*(4), 1955–1963. https://doi.org/10.1021/es2019675

González-Gaya, B., Fernández-Pinos, M.-C., Morales, L., Méjanelle, L., Abad, E., Piña, B., et al. (2016). High atmosphere–ocean exchange of semivolatile aromatic hydrocarbons. *Nature Geoscience*, *9*, 438–442.

González-Gaya, B., Martínez-Varela, A., Vila-Costa, M., Casal, P., Cerro-Gálvez, E., Berrojalbiz, N., et al. (2019). Biodegradation as an important sink of aromatic hydrocarbons in the oceans. *Nature Geoscience*, *12*, 119–125.

Gorman, A. A., & Rodgers, M. A. J. (1989). In J. C. Scaiano (Ed.), *Handbook or organic photochemistry* (Vol. 2, pp. 229–247). Boca Raton, FL: CRC Press.

Grossman, J. N., Stern, A. P., Kirich, M. L., & Kahan, T. F. (2016). Anthracene and pyrene photolysis kinetics in aqueous, organic, and mixed aqueous-organic phases. *Atmospheric Environment*, *128*, 158–164.

Guigue, C., Tedetti, M., Giorgi, S., & Goutx, M. (2011). Occurrence and distribution of hydrocarbons in the surface microlayer and subsurface water from the urban coastal marine area off Marseilles, Northwestern Mediterranean Sea. *Marine Pollution Bulletin*, *62*(12), 2741–2752. https://doi.org/10.1016/j.marpolbul.2011.09.013

Han, C., Liu, Y., Ma, J., & He, H. (2012). Key role of organic carbon in the sunlight-enhanced atmospheric aging of soot by O2. *Proceedings of the National Academy of Sciences of the United States of America*, *109*, 21250–21255.

Hardy, J. T., Crecelius, E. A., Antrim, L. D., Kiesser, S. L., & Broadhurst, V. L. (1990). Aquatic surface microlayer contamination in Chesapeake Bay. *Marine Chemistry*, *28*, 333–351.

Hersey, S. P., Sorooshian, A., Murphy, S. M., Flagan, R. C., & Seinfeld, J. H. (2009). Aerosol hygroscopicity in the marine atmosphere: A closure study using high-time-resolution, multiple-RH DASH-SP and size-resolved C-ToF-AMS data. *Atmospheric Chemistry and Physics*, *9*, 2543–2554.

Hoffmann, E. H., Tilgner, A., Schrödner, R., Bräuer, P., Wolke, R., & Herrmann, H. (2016). An advanced modeling study on the impacts and atmospheric implications of multiphase dimethyl sulfide chemistry. *Proceedings of the National Academy of Sciences of the United States of America*, *113*, 11776–11781.

Hsu, W. T., Liu, M. C., Hung, P. C., Chang, S. H., & Chang, M. B. (2016). PAH emissions from coal combustion and waste incineration. *Journal of Hazardous Materials*, *318*, 32–40. https://doi.org/10.1016/j.jhazmat.2016.06.038

Stewart, J. J. P. MOPAC2016 (Version 17.181), (2016). Stewart computational chemistry, web-site: HTTP://OpenMOPAC.net.

Huang, X.-D., Dixon, D. G., & Greenberg, B. M. (1993). Impacts of UV radiation and photomodification on the toxicity of PAHs to the higher plant Lemna gibba (Duckweed). *Environmental Toxicology and Chemistry*, *12*, 1067–1077.

Jiang, B., Kuang, B. Y., Liang, Y. M., Zhang, J. Y., Huang, X. H. H., Xu, C. M., et al. (2016). Molecular composition of urban organic aerosols on clear and hazy days in Beijing: A comparative study using FT-ICR MS. *Environmental Chemistry*, *13*, 888–901.

Jiang, B., Liang, Y. M., Xu, C. M., Zhang, J. Y., Hu, M., & Shi, Q. (2014). Polycyclic aromatic hydrocarbons (PAHs) in ambient aerosols from Beijing: Characterization of low volatile PAHs by positive-ion atmospheric pressure photoionization (APPI) coupled with Fourier Transform Ion Cyclotron Resonance. *Environmental Science and Technology*, *48*(9), 4716–4723. https://doi.org/10.1021/es405295p

Keyte, I. J., Harrison, R. M., & Lammel, G. (2013). Chemical reactivity and long-range transport potential of polycyclic aromatic hydrocarbons—A review. *Chemical Society Reviews*, *42*(24), 9333–9391. https://doi.org/10.1039/c3cs60147a

Kim, S., Kramer, W. R., & Hatcher, G. P. (2003). Graphical method for analysis of ultrahigh-resolution broadband mass spectra of natural organic matter, the Van Krevelen diagram. *Analytical Chemistry*, *75*, 5336–5344.

Kinani, S., Bouchonnet, S., Creusot, N., Bourcier, S., Balaguer, P., Porcher, J. M., & Aït-Aïssa, S. (2010). Bioanalytical characterisation of multiple endocrine-anddioxin-like activities in sediments from reference and impacted small rivers. *Environmental Pollution*, *158*(1), 74–83. https://doi.org/10.1016/j.envpol.2009.07.041

Kinani, S., Soussi, Y., Kinani, A., Vujovic, S., Aït-Aïssa, S., & Bouchonnet, S. (2016). Photodegradation of fluorene in aqueous solution: Identification and biological activity testing of degradation products. *Journal of Chromatography A*, *1442*, 118–128. https://doi.org/10.1016/j.chroma.2016.03.012

Kourtchev, I., O'Connor, I. P., Giorio, C., Fuller, S. J., Kristensen, K., Maenhaut, W., et al. (2014). Effects of anthropogenic emissions on the molecular composition of urban organic aerosols: An ultrahigh resolution mass spectrometry study. *Atmospheric Environment*, *89*, 525–532.

Kuang, B. Y., Lin, P., Hu, M., & Yu, J. Z. (2016). Aerosol size distribution characteristics of organosulfates in the Pearl River Delta region, China. *Atmospheric Environment*, *130*, 23–35.

Legrand, M., Sciare, J., Jourdain, B., & Genthon, C. (2011). Subdaily variations of atmospheric dimethylsulfide, dimethylsulfoxide, methanesulfonate, and non-sea-salt sulfate aerosols in the atmospheric boundary layer at Dumont d'Urville (coastal Antarctica) during summer. *Journal of Geophysical Research*, *106*, D15205. https://doi.org/10.1029/2000JD900840

Li, T., Pan, D., Bai, Y., Li, G., He, X., Chen, A. C.-T., et al. (2015). Satellite remote sensing of ultraviolet irradiance on the ocean surface. *Acta Oceanologica Sinica*, *34*, 101–112.

Librando, V., Bracchitta, G., de Guidi, G., Minniti, Z., Perrini, G., & Catalfo, A. (2014). Photodegradation of anthracene and benzo[a]-anthracene in polar and apolar media: New pathways of photodegradation. *Polycyclic Aromatic Compounds*, *34*(3), 263–279.

Lim, L., Wurl, O., Karuppiah, S., & Obbard, J. (2007). Atmospheric wet deposition of PAHs to the sea-surface microlayer. *Marine Pollution Bulletin*, *54*(8), 1212–1219. https://doi.org/10.1016/j.marpolbul.2007.03.023

Lin, P., Rincon, A. G., Kalberer, M., & Yu, J. C. (2012). Elemental composition of HULIS in the Pearl River Delta Region, China: Results inferred from positive and negative electrospray high resolution mass spectrometric data. *Environmental Science and Technology*, *46*(14), 7454–7462. https://doi.org/10.1021/es300285d

Liss, S. P., & Duce, R. A. (1997). *The sea surface and global change*. Cambridge: University Press.

Liu, K., & Dickhut, R. M. (1997). Surface microlayer enrichment of polycyclic aromatic hydrocarbons in Southern Chesapeake Bay. *Environmental Science and Technology*, *31*, 2777–2781.

Lohmann, R., Gioia, R., Jones, K. C., Nizzetto, L., Temme, C., Xie, Z., et al. (2009). Organochlorine pesticides and PAHs in the surface water and atmosphere of the North Atlantic and Arctic Ocean. *Environmental Science and Technology*, *43*(15), 5633–5639. https://doi.org/10.1021/es901229k

Ma, Y., Xie, Z., Yang, H., Möller, A., Halsall, C., Cai, M., et al. (2013). Deposition of polycyclic aromatic hydrocarbons in the North Pacific and the Arctic. *Journal of Geophysical Research: Atmosphere*, *118*, 5822–5829. https://doi.org/10.1002/jgrd.50473

Manodori, L., Gambaro, A., Piazza, R., Ferrari, S., Stortini, A. M., Moret, I., & Capodaglio, G. (2006). PCBs and PAHs in sea-surface microlayer and sub-surface water samples of the Venice Lagoon (Italy). *Marine Pollution Bulletin*, *52*(2), 184–192. https://doi.org/10.1016/j.marpolbul.2005.08.017

Mekic, M., Liu, J., Zhou, W., Loisel, G., Cai, J., He, T., et al. (2019). Formation of highly oxygenated multifunctional compounds from cross-reactions of carbonyl compounds in the atmospheric aqueous phase. *Atmospheric Environment*, *219*. https://doi.org/10.1016/j.atmosenv.2019.117046

Mekic, M., Loisel, G., Zhou, W., Jiang, B., Vione, D., & Gligorovski, S. (2018). Ionic strength effects on the reactive uptake of ozone on aqueous pyruvic acid: Implications for air-sea ozone deposition. *Environmental Science and Technology*, *52*(21), 12306–12315. https://doi.org/10.1021/acs.est.8b03196

Monge, M. E., D'Anna, B., Mazri, L., Giroir-Fendler, A., Ammann, M., Donaldson, D. J., & George, C. (2010). Light changes the atmospheric reactivity of soot. *Proceedings of the National Academy of Sciences of the United States of America*, *107*, 6605–6609.

Nizkorodov, S. A., Laskin, J., & Laskin, A. (2011). Molecular chemistry of organic aerosols through the application of high resolution mass spectrometry. *Physical Chemistry Chemical Physics*, *13*, 3561–4164.

O'Dowd, C. D., Facchini, M. C., Cavalli, F., Ceburnis, D., Mircea, M., Decesari, S., et al. (2004). Biogenically driven organic contribution to marine aerosol. *Nature*, *431*(7009), 676–680. https://doi.org/10.1038/nature02959

Otto, S., Streibel, T., Erdmann, S., Klingbeil, S., Schulz-Bull, D., & Zimmermann, R. (2015). Pyrolysis-gas chromatography-mass spectrometry with electronionization or resonance-enhanced-multi-photon-ionization for characterization of polycyclic aromatic hydrocarbons in the Baltic Sea. *Marine Pollution Bulletin*, *99*(1-2), 35–42. https://doi.org/10.1016/j.marpolbul.2015.08.001

Pérez-Cerrera, E., León, V. M., Parra, A. G., & González-Mazo, E. (2007). Simultaneous determination of pesticides polycyclic aromatic hydrocarbons and polychlorinated biphenyls in seawater and interstitial marine water samples, using stir bar sorptive extraction-thermal desorption-gas chromatography-mass spectrometry. *Journal of Chromatography A*, *1170*, 82–90.

Ravindra, K., Sokhi, R., & Van Grieken, R. (2008). Atmospheric polycyclic aromatic hydrocarbons: Source attribution, emission factors and regulation. *Atmospheric Environment*, *42*, 2895–2921.

Rincon, A. G., Calvo, A. I., Dietzel, M., & Kalberer, M. (2012). Seasonal differences of urban organic aerosol composition-an ultra-high resolution mass spectrometry study. *Environmental Chemistry*, *9*, 298–319.
Seidel, M., Manecki, M., Herlemann, D. P. R., Deutsch, B., Schulz-Bull, D., Jürgens, K., & Dittmar, T. (2017). Composition and transformation of dissolved organic matter in the Baltic Sea. *Frontiers in Earth Science*, *5*(31). https://doi.org/10.3389/feart.2017.00031
Sepic, E., Bricelj, M., & Leskovsek, H. (2003). Toxicity of fluoranthene and its biodegradation metabolites to aquatic organisms. *Chemosphere*, *52*(7), 1125–1133. https://doi.org/10.1016/S0045-6535(03)00321-7
Simo, R., & Vila-Costa, M. (2006). Ubiquity of algal dimethylsulfoxide in the surface ocean: Geographic and temporal distribution patterns. *Marine Chemistry*, *100*, 136–146.
Spranger, T., van Pinxteren, D., Reemtsma, T., Lechtenfeld, O. J., & Herrmann, H. (2019). 2-D liquid chromatographic fractionation with ultra-high resolution MS analysis resolves a vast molecular diversity of tropospheric particle organics. *Environmental Science and Technology*, *53*(19), 11353–11363. https://doi.org/10.1021/acs.est.9b03839
Stewart, J. J. P. (2013). Optimization of parameters for semiempirical methods VI: More modifications to the NDDO approximations and re-optimization of parameters. *Journal of Molecular Modelling*, *19*, 1–32.
Stirchak, L. T., Moor, K. J., McNeill, K. D., & Donaldson, J. (2019). Differences In Photochemistry Between Seawater And Freshwater For Two Natural Organic Matter Samples. *Environmental Science: Processes & Impacts*, *21*, 28–39.
Stortini, A. M., Martellini, T., Del Bubba, M., Lepri, L., Capodaglioc, G., & Cincinelli, A. (2009). n-Alkanes, PAHs and surfactants in the sea surface microlayer and sea water samples of the Gerlache Inlet Sea (Antarctica). *Microchemical Journal*, *92*, 37–43.
Styler, S. A., Loiseaux, M. E., & Donaldson, D. J. (2011). Substrate effects in the photoenhanced ozonation of pyrene. *Atmospheric Chemistry and Physics*, *11*, 1243–1253.
Tao, S., Lu, X., Levac, N., Bateman, A. P., Nguyen, T. B., Bones, D. L., et al. (2014). Molecular characterization of organosulfates in organic aerosols from Shanghai and Los Angeles urban areas by nanospray-desorption electrospray ionization high-resolution mass spectrometry. *Environmental Science and Technology*, *48*, 10993–11001.
Tubaro, M., Marotta, E., Seraglia, R., & Traldi, P. (2003). Atmospheric pressure photoionization mechanisms. The case of benzene and toluene. *Rapid Communications in Mass Spectrometry*, *17*(21), 2423–2429. https://doi.org/10.1002/rcm.1208
Vacha, R., Jungwirth, P., Chen, J., & Valsaraj, K. (2006). Adsorption of polycyclic aromatic hydrocarbons at the air-water interface: Molecular dynamics simulations and experimental atmospheric observations. *Physical Chemistry Chemical Physics*, *8*(38), 4461–4467. https://doi.org/10.1039/b610253k
Valavanidis, A., Vlachogianni, T., Triantafillaki, S., Dassenakis, M., Androutsos, F., & Scoullos, M. (2008). Polycyclic aromatic hydrocarbons in surface seawater and in indigenous mussels (Mytilus galloprovincialis) from coastal areas of the Saronikos Gulf (Greece). *Estuarine Coastal and Shelf Science*, *79*, 733–739.
Vasilkov, A., Krotkov, N., Herman, J., McClain, C., Arrigo, K., & Robinson, W. (2001). Global mapping of underwater UV irradiances and DNA-weighted exposures using total ozone mapping spectrometer and sea-viewing wide field of-view sensor data products. *Journal of Geophysical Research*, *106*(C11), 27205–27219.
Veljković, D. Ž. (2018). Strong CH/O interactions between polycyclic aromatic hydrocarbons and water: Influence of aromatic system size. *Journal of Molecular Graphics and Modelling*, *80*, 121–125. https://doi.org/10.1016/j.jmgm.2017.12.014
Vione, D., Albinet, A., Barsotti, F., Mekic, M., Jiang, B., Minero, C., et al. (2019). Formation of substances with humic-like fluorescence properties, upon photoinduced oligomerization of typical phenolic compounds emitted by biomass burning. *Atmospheric Environment*, *206*, 197–207.
Wang, K., Zhang, Y., Huang, R.-J., Cao, J., & Hoffmann, T. (2018). UHPLC-Orbitrap mass spectrometric characterization of organic aerosol from a central European city (Mainz, Germany) and a Chinese megacity (Beijing). *Atmospheric Environment*, *189*, 22–29.
Wang, X., Hayeck, N., Brüggemann, M., Yao, L., Chen, H., Zheng, C., et al. (2017). Chemical characteristics of organic aerosols in shanghai: A study by ultra-high-performance liquid chromatography coupled with Orbitrap mass spectrometry. *Journal of Geophysical Research: Atmosphere*, *122*, 11,703–11,722. https://doi.org/10.1002/2017JD026930
Wang, X. K., Rossignol, S., Ma, Y., Yao, L., Wang, M. Y., Chen, J. M., et al. (2016). Molecular characterization of atmospheric particulate organosulfates in three megacities at the middle and lower reaches of the Yangtze River. *Atmospheric Chemistry and Physics*, *16*, 2285–2298.
Wilkinson, F., Helman, W. P., & Ross, A. B. (1995). Rate constants for the decay and reactions of the lowest electronically excited singlet state of molecular oxygen in solution. An expanded and revised compilation. *Journal of Physical and Chemical Reference Data*, *24*, 663.
Wu, Z., Rodgers, R. P., & Marshall, A. G. (2004). Two- and three-dimensional van Krevelen Diagrams: A graphical analysis complementary to the Kendrick mass plot for sorting elemental compositions of complex organic mixtures based on ultrahigh-resolution broadband Fourier transform ion cyclotron resonance mass measurements. *Analytical Chemistry*, *76*(9), 2511–2516. https://doi.org/10.1021/ac0355449
Wurl, O., Werner, E., Landing, W. M., & Zappa, C. J. (2011). Sea surface microlayer in a changing ocean—A perspective. *Elementa: Science of the Anthropocene*, *5*, 31–42.
Yassine, M. M., Harir, M., Dabek-Zlotorzynska, E., & Schmitt-Kopplin, P. (2014). Structural characterization of organic aerosol using Fourier transform ion cyclotron resonance mass spectrometry: Aromaticity equivalent approach. *Rapid Communication in Mass Spectrometry*, *28*, 2445–2454.
Zelenyuk, A., Imre, D. G., Wilson, J., Bell, D. M., Suski, K. J., Shrivastava, M., et al. (2017). The effect of gas-phase polycyclic aromatic hydrocarbons on the formation and properties of biogenic secondary organic aerosol particles. *Faraday Discussions*, *200*, 143–164. https://doi.org/10.1039/c7fd00032d
Zeng, J., Yu, Z., Mekic, M., Liu, J., Li, S., Loisel, G., et al. (2020). Evolution of indoor cooking emissions captured by using secondary electrospray ionization high-resolution mass spectrometry. *Environmental Science and Technology Letters*, *7*(2), 76–81. https://doi.org/10.1021/acs.estlett.0c00044
Zhou, S., Hwang, B. C. H., Lakey, P. S. J., Zuend, A., Abbatt, J. P. D., & Shiraiwa, M. (2019). Multiphase reactivity of polycyclic aromatic hydrocarbons is driven by phase separation and diffusion limitations. *Proceedings of the National Academy of Sciences of the United States of America*, *116*, 11658–11663.